JOURNAL OF SOLID STATE CHEMISTRY 96, 227–236 (1992)

The Magnetic Structure of Cr_2F_5

P. LACORRE AND G. FEREY

Laboratoire des Fluorures, U.R.A. C.N.R.S. 449, Université du Maine, Avenue Olivier-Messiaen, 72017 Le Mans Cedex, France

AND J. PANNETIER

Institut Laue Langevin, 156X, Avenue des Martyrs, 38042 Grenoble Cedex, France

Received July 12, 1991

The magnetic structure of Cr_2F_5 has been determined by means of neutron powder diffraction. It is antiferromagnetic, with magnetic space group $C2/c$, the same as the crystal space group. Magnetic moments lie mainly in the (**a, c**) plane, mostly along the **a** axis. The observed magnetic structure does not correspond to previous predictions. New superexchange mechanisms are proposed, which take into account the specific superexchange angles. They are in agreement with the rules for superexchange coupling, the Jahn–Teller effect, and the magnetic properties of the compound. Monte Carlo simulations show that the proposed superexchange interactions are consistent with the magnetic structure.

1. Introduction

As a contribution to a series of papers about ordered magnetic frustration in fluorides, we previously determined the magnetic structure of $\alpha KCrF_4$, which exhibits triangular platelets of magnetic cations (Cr^{III}) in antiferromagnetic interaction (*1*, *2*). In the present paper, we focus on another chromium fluoride with a pseudo-triangular (hexagonal) magnetic sublattice, which involves both Cr^{II} and Cr^{III} cations.

Cr_2F_5 has been isolated for the first time by Sturm (*3*) and its crystal structure has been determined by Steinfink and Burns (*4*). It crystallizes in a monoclinic cell, space group $C2/c$, with room temperature cell parameters $a = 7.773(5)$ Å, $b = 7.540(5)$ Å, $c = 7.440(5)$ Å, $\beta = 124.25(1)°$ ($Z = 4$).

The crystal structure is shown in Fig. 1. It is built up from rows of edge-sharing $[Cr^{II}F_6]$ octahedra (as in rutile CrF_2) connected to rows of corner-sharing $[Cr^{III}F_6]$ octahedra (as in perovskite CrF_3). Each octahedral row is connected by corners to four octahedral rows of the other species, resulting in a pseudo-hexagonal cationic sublattice. The coordination polyhedron of chromium II is strongly deformed by the Jahn–Teller effect, with two long distances (twice 2.57 Å) due to half-filled d_{z^2} orbitals of Cr^{II}.

If superexchange coupling in Cr^{III} fluorides is now fairly well documented, this is not the case for Cr^{II} fluorides, mostly because of the lack of reference compounds. The superexchange mechanisms involved through the different Cr^{II} orbitals seem to be clear for 180°-type configuration, leading

0022-4596/92 $3.00

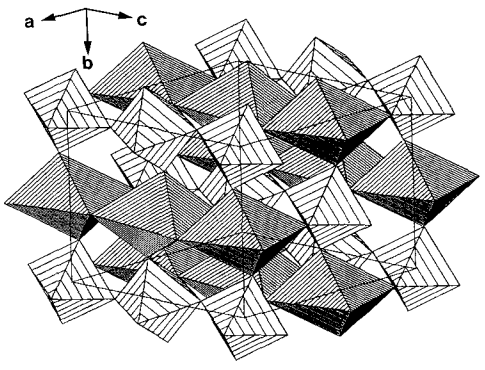

FIG. 1. Crystal structure of Cr_2F_5 (from (*13*)). Chromium (II) coordination octahedra are more heavily hatched than chromium (III) ones.

to F or AF interactions depending whether half-filled d_{z^2} orbitals are or are not involved in the bonding. This point has been evidenced experimentally in the perovskite $KCrF_3$ (*5*) and a theoretical explanation has been given (*6*). The situation is less clear when superexchange configuration is not of a pure 180° type. For instance, the rutile CrF_2 has a spin configuration (*7*) very similar to that of most other transition metal difluorides (*8–11*), at variance with that of another Jahn–Teller cation difluoride CuF_2 (*12*). Cr_2F_5, another Cr^{II} fluoride with superexchange configurations different from the pure 180° type, has been used as a test example for coupling mechanisms. Magnetic models have been proposed (*13, 14*), whose validity has not been questioned so far because the magnetic structure of the compound was not actually known.

In this paper we present the magnetic structure of Cr_2F_5 as determined from neutron powder diffraction data. The refined spin arrangement does not correspond to the models suggested previously, thus questioning the suggested superexchange mechanisms. We propose new mechanisms for two superexchange interactions, whose consistency with the magnetic structure is shown by means of Monte Carlo simulations.

2. Experimental

A powdered sample of Cr_2F_5 was synthesized by heating a stoichiometric mixture of CrF_2 and CrF_3 in a sealed platinum tube under argon atmosphere for 20 hr at 840°C. CrF_2 was prepared from a stoichiometric mixture of powdered samples of CrF_3 and metallic chromium, heated under argon atmosphere in a sealed platinum tube at 950°C for 12hr. CrF_3 was obtained by fluorinating a commercial sample (Merck) of $CrCl_3$.

Neutron diffraction patterns were collected on the powder diffractometer D1A ($\lambda = 1.909$ Å, $0° < 2\theta < 160°$) of the Institut Laue Langevin in Grenoble. The powdered sample was contained in a cylindrical vanadium can ($\phi = 15$ mm) placed in a liquid helium cryostat with temperature regulation.

The diffraction patterns were analyzed by using the Rietveld method (*15*) as modified by Hewat (*16*). The scattering lengths and magnetic form factors were taken from Refs. (*17*) and (*18*), respectively. Bertaut's macroscopic theory (*19*) was used to determine the magnetic coupling modes.

3. Magnetic Structure at 2 K

Magnetic susceptibility curves show that Cr_2F_5 orders antiferromagnetically below $T_N = 40$ K (*14*). Two diffraction patterns were recorded above (61 K) and below (2 K) the ordering temperature. The 61-K neutron diffraction pattern was consistent with the room temperature crystal structure determined by Steinfink and Burns (*4*).

The 2-K pattern exhibits new diffraction peaks as well as a (sometimes very strong) increase in the intensity of some of the high temperature, purely nuclear, peaks. Every new reflection is compatible with the crystal

TABLE I

COORDINATES OF MAGNETIC CATIONS Cr^{III} (SITE 4*a*) IN SPACE GROUP *C*2/*c*

	Atomic coordinates		
Spins	*x*	*y*	*z*
S_1	0	0	0
S_2	0	0	$\frac{1}{2}$
S_3	$\frac{1}{2}$	$\frac{1}{2}$	0
S_4	$\frac{1}{2}$	$\frac{1}{2}$	$\frac{1}{2}$

Note. Atomic coordinates of Cr^{II} (site 4*b*) are deduced by a translation [0, $\frac{1}{2}$, 0].

cell and with space group *C*2/*c*. Therefore, we determined the possible coupling modes by applying Bertaut's macroscopic theory (*19*) to this space group. Chromium atoms are located on special positions 4*a* (Cr^{II}) and 4*b* (Cr^{III}) of the space group. The lattice translation **C** [$\frac{1}{2}$, $\frac{1}{2}$, 0], the screw axis $\mathbf{2_{1y}}$, and the inversion center $\bar{\mathbf{1}}$ were chosen as independent symmetry elements.

Let S_i ($i = 1, 4$) be the magnetic moments carried by atoms whose positions are given in Table I. The base vectors, built from linear combination of these moments, are:

$$F = S_1 + S_2 + S_3 + S_4$$
$$G = S_1 - S_2 + S_3 - S_4$$
$$C = S_1 + S_2 - S_3 - S_4$$
$$A = S_1 - S_2 - S_3 + S_4.$$

The inversion center $\bar{\mathbf{1}}$ leaves these moments unchanged. Table II gives the four

TABLE II

IRREDUCIBLE REPRESENTATIONS OF MAGNETIC MOMENTS OF CHROMIUM CATIONS IN SPACE GROUP *C*2/*c*

Modes	*x*	*y*	*z*
$\Gamma_1(++)$	G_x	F_y	G_z
$\Gamma_2(+-)$	F_x	G_y	F_z
$\Gamma_3(-+)$	C_x	A_y	C_z
$\Gamma_4(--)$	A_x	C_y	A_z

representations compatible with the space group *C*2/*c*. Two of them are purely antiferromagnetic (Γ_3 and Γ_4). They correspond to the magnetic models previously proposed for the magnetic structure of Cr_2F_5 (*13, 14*). It can be shown that representations Γ_3 and Γ_4 do generate magnetic reflections which are independent from the nuclear reflections. This is at variance with experimental observation, thus ruling out those representations and the corresponding models as possible magnetic structures for Cr_2F_5. Further refinements show that the spin arrangement in Cr_2F_5 corresponds to the representation Γ_1 (G_x, F_y, G_z), that is, to the magnetic space group *C*2/*c*.

The best reliability factors (R_I = 0.051 (R_{nuc} = 0.047 and R_{mag} = 0.074), R_p = 0.090, R_{wp} = 0.103) were obtained for the values of atomic positions and magnetic moments given in Table III. In this table we also added, for comparison, the room temperature atomic positions as determined by Steinfink and Burns from single crystal data. The low and room temperature values are very close to each other. Table IV gives a selection of interatomic distances and angles, which are of interest in relation with the magnetic coupling mechanisms. Observed and calculated profiles are given in Fig. 2.

The Cr^{II} and Cr^{III} spin sublattices, since they are deduced from each other by a translation, are indistinguishible by nonpolarized neutron diffraction. We chose the attribution which seems the most reasonable given the spin amplitudes and the electronic configurations of Cr^{II} and Cr^{III}.

The projection of the magnetic structure on the (**a, c**) plane is shown in Fig. 3. The ferromagnetic components of spins along the **b** axis are at the most very weak (the remanent magnetization is not significantly different from zero). In the (**a, c**) plane, the magnetic moments are almost exactly aligned with the **a** axis. The spin arrange-

TABLE III

CRYSTAL AND MAGNETIC STRUCTURE OF Cr_2F_5 AT 2 K FROM NEUTRON POWDER DIFFRACTION

	Atomic positions				Magnetic moments (μB)			
Atoms	x	y	z	B(Å^2)	M_x	M_y	M_z	M_{tot}
Cr^{III}	0	0	0	0.21(6)	2.19(5)	−0.33(32)	−0.70(8)	2.66(9)
Cr^{II}	0	$\frac{1}{2}$	0	0.19(7)	−3.67(6)	0.59(32)	−0.23(10)	3.59(9)
F1	0	0.0530(3) [0.0475(7)]	$\frac{1}{4}$	0.55(5)				
F2	0.2967(3) [0.2955(5)]	0.9773(2) [0.9808(5)]	0.1759(3) [0.1762(6)]	0.33(4)				
F3	0.0235(3) [0.0207(6)]	0.2454(3) [0.2448(4)]	0.9667(3) [0.9696(6)]	0.39(3)				

Note. In brackets: crystal structure at room temperature, from (*4*)). a = 7.7526(1) [7.773(5)] Å, b = 7.5228(1) [7.540(5)] Å, c = 7.4477(1) [7.440(5)] Å, β = 124.081(1) [124.25(1)]°. Space group: $C2/c$.

ment is strictly AF within each kind of (rutile and perovskite) row of octahedra. It is also AF from one type of row to the other along the **b** axis.

As the spin direction in Cr_2F_5 is most probably governed by the anisotropic d^4 Cr^{II} cations, a comparison can be made with that of CrF_2: the angle between the spin orientation and the rutile chains axis is 32° in CrF_2 and about 55° in Cr_2F_5. The major difference between the two spin arrangements within the rutile chains is that one is F (CrF_2) while the other is AF (Cr_2F_5). As noted in Ref. (*14*), this should not be considered as very surprising since the Cr^{II}–F–Cr^{II} interaction in the rutile chain is so weak that the spin arrangement is most probably ruled by the Cr^{II}–F–Cr^{III} interactions (see Section 5).

In the next section, we shall examine in more detail the superexchange interactions in the compound by means of Monte Carlo simulations and in relation to the proposed models.

TABLE IV

SELECTION OF INTERATOMIC DISTANCES (Å) AND ANGLES (°) IN Cr_2F_5 AT 2 K

Chromium coordination octahedra		
Cr^{III}–F1	2 × 1.904(1) [1.894(2)]	
Cr^{III}–F2	2 × 1.913(2) [1.904(4)]	
Cr^{III}–F3	2 × 1.885(2) [1.877(3)]	
Cr^{II}–F2	2 × 2.558(3) [2.572(4)]	
Cr^{II}–F2	2 × 2.019(2) [2.010(5)]	
Cr^{II}–F3	2 × 1.953(2) [1.955(4)]	
Superexchange angles[a]		
Cr^{II}–F2–Cr^{II}	108.3(1) [107.9(2)]	(J_1)
Cr^{III}–F1–Cr^{III}	155.8(2) [158.2(3)]	(J_2)
Cr^{II}–F2–Cr^{III}	119.5(1) [119.8(2)]	(J_3)
Cr^{II}–F2–Cr^{III}	130.2(2) [130.8(3)]	(J_4)
Cr^{II}–F3–Cr^{III}	157.1(2) [159.3(3)]	(J_5)

Note. In brackets: at room temperature from (*13*).

[a] In the last column figure the corresponding superexchange interactions as numbered in Sections 4 and 5.

4. Monte Carlo Simulations

The cationic sublattice of Cr_2F_5 is topologically simple since it corresponds to an ordered distribution of Cr^{II} and Cr^{III} cations on a pseudo-hexagonal sublattice (see Fig. 4). The interaction network is more complex, and five different types of superexchange interactions have been considered (for the sake of clarity we keep here the numbering of Ref. (*14*)):

J_1 = direct coupling and 108° Cr^{II}–F–Cr^{II} superexchange coupling within rutile chains (edge-sharing along **c**),

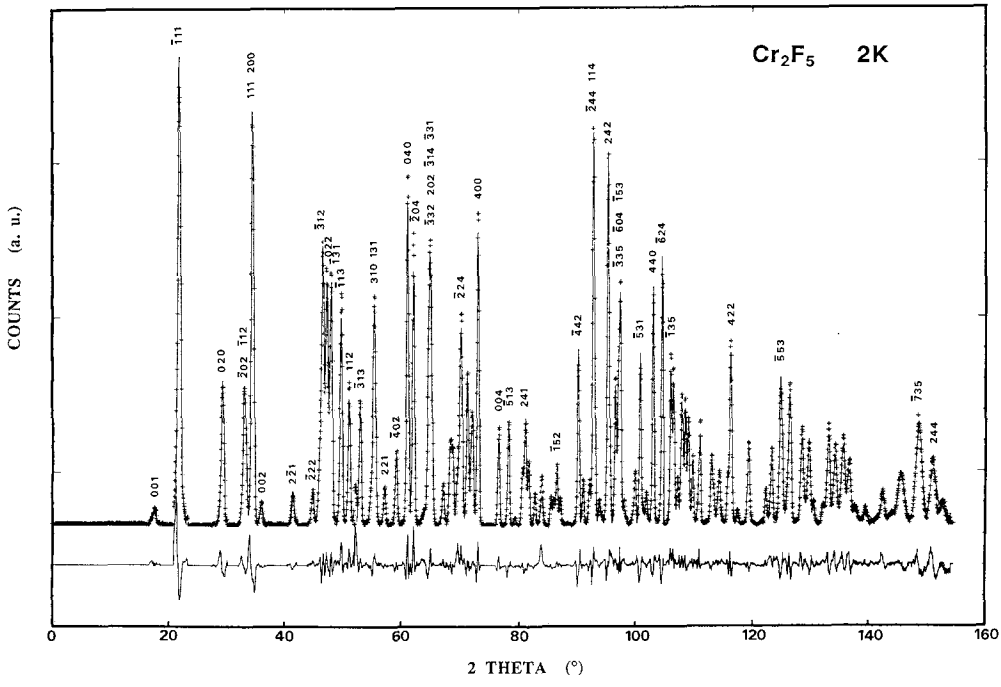

FIG. 2. Observed (crosses) and calculated (lines) neutron diffraction profiles of Cr_2F_5 at 2 K. The difference pattern at the same scale is shown at the bottom part of the figure.

J_2 = 156° Cr^{III}–F–Cr^{III} superexchange coupling within perovskite rows (corner-sharing along **c**),

J_3 = 120° Cr^{II}–F–Cr^{III} superexchange coupling along **a**),

J_4 = 130° Cr^{II}–F–Cr^{III} superexchange coupling along [101],

J_5 = 157° Cr^{II}–F–Cr^{III} superexchange coupling along **b**.

The possible signs of these interactions have been analyzed in detail in Refs. (*13*) and (*14*), which conclude identical models.

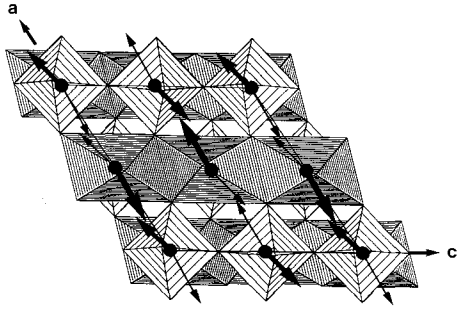

FIG. 3. Projection of the magnetic structure of Cr_2F_5 on the (**a**, **c**) plane. Thick arrows represent magnetic moments carried by atoms in the front layer of the figure.

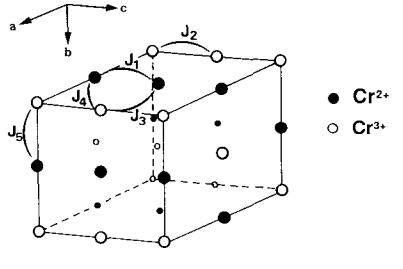

FIG. 4. Magnetic sublattice of Cr_2F_5. Black and open circles represent Cr^{II} and Cr^{III} cations, respectively.

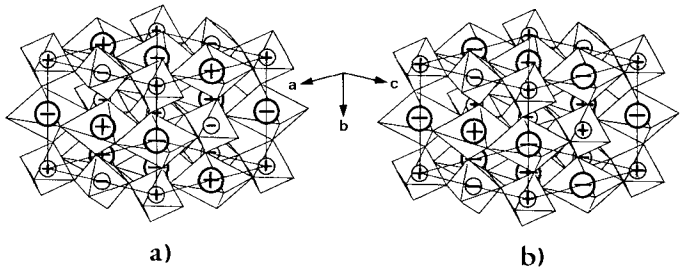

FIG. 5. Relative spin orientation: a) in the model proposed by Osmond (*13*) and Tressaud *et al.* (*14*), b) in the observed magnetic structure of Cr_2F_5.

Their conclusions about the sign of the interactions are the following:

J_1 should be very weak and negligible compared to the other interactions because of a compensation of F and AF superexchange mechanisms. All other interactions should be AF except J_3, which is expected to be F.

When the magnetic structure of Cr_2F_5 is compared with the predicted one (see Fig. 5), it can be seen that part of the predictions is not verified. The incriminated coupling constants are J_3 and J_4: spins order in a direction opposite to that they should have if J_3 and J_4 were F and AF, respectively. Therefore, it seems that the sign of at least one of these interactions should be reconsidered in order to agree with the observed magnetic structure.

In order to check the stability range of a Cr_2F_5-type magnetic structure with respect to the two coupling constants, we explored the corresponding phase diagram by Monte Carlo simulation. For this purpose we used the computer program MCMAG (*20*), whose algorithm and some applications have been described elsewhere (*21*). As exploring the 5D-space of the coupling constants phase diagram was excluded on the basis of the CPU time it would require (and not very interesting anyway), we focused on the questioned coupling constants J_3 and J_4.

For the series of simulations, J_1 was held fixed to zero, since it is expected to be negligible, and antiferromagnetic J_2 and J_5 were set to the arbitrary value of -10K (the strength of J_5 does not influence the ground-state magnetic structure, as far as it remains AF). Only J_3 and J_4 were varied, allowing us to explore the J_3–J_4 phase diagram. A total of 46 points in this phase diagram were effectively simulated, only in the frustrated parts of the diagram (in nonfrustrated magnetic structures, the spin arrangement follows the sign of interactions). A 128-spin sample of 16 unit cells ($4\mathbf{a} \times \mathbf{b} \times 4\mathbf{c}$) was used for each simulation, with free edges in order to avoid artificial constraints due to periodic boundary conditions. The spin amplitudes were set to 3 and 4 μB for Cr^{III} and Cr^{II}, respectively, and XY-type spins were used. The cooling schedule followed a geometric law with multiplicative factor 0.9 from $T_{ini} = 100$ K to $T_{fin} = 0.5$ or 0.1 K, depending on the position in the phase diagram. At each temperature, 400 or 700 Monte Carlo cycles per spin were performed.

The results of the simulation are summarized in Fig. 6. Two quadrants (upper left and lower right) correspond to unfrustrated interactions, the two others being frustrated. Four different types of collinear spin arrangements (called I, II, III, and IV) were found, two of them being always frustrated (III and IV). The other two collinear configurations correspond to the magnetic structure of Cr_2F_5 (I) and to the isotropic

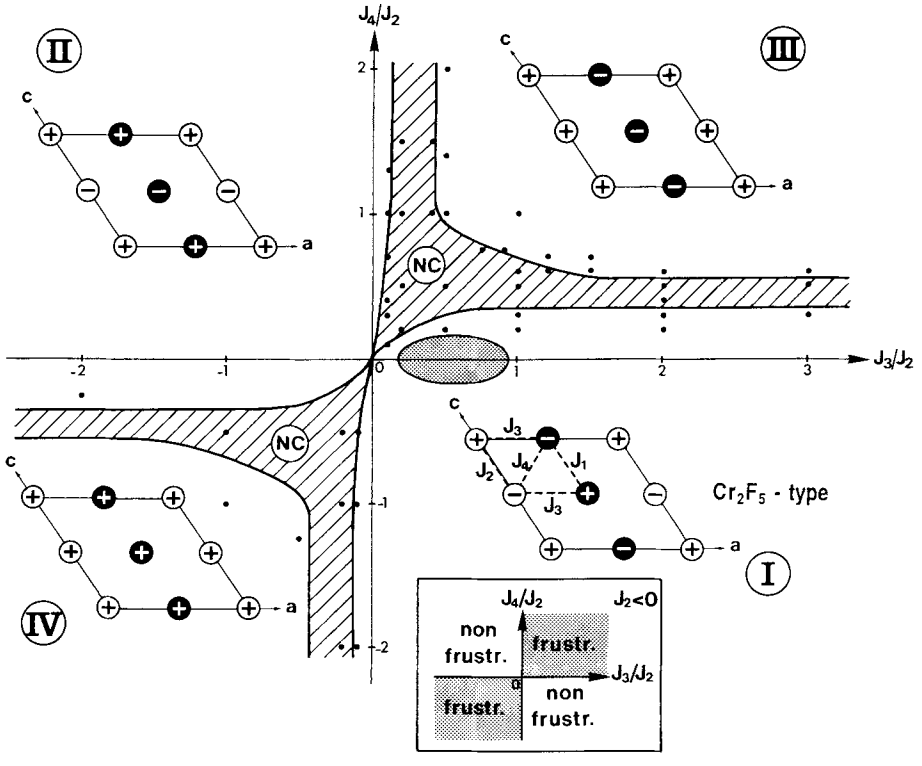

FIG. 6. Approximate phase diagram of a Cr_2F_5-type lattice in the J_3—J_4 plane from Monte Carlo simulation results (J_2 antiferromagnetic). Dots represent systems that were effectively simulated. The hatched area corresponds to noncollinear (NC) magnetic structures (the lower left part of this area has been deduced from the upper right part by symmetry). In the displayed collinear spin configurations, black and open circles represent Cr^{II} and Cr^{III} cations, respectively. The point representative of Cr_2F_5 should lie inside the shaded oval region, approximately (see Section 5). In inset: frustrated and nonfrustrated quadrants of the phase diagram.

models given in Refs. (*13*) and (*14*) (II). The regions at the border of these collinear structures (hatched area of Fig. 6) are characterized by noncollinear spin arrangements.

An interesting result of these simulations is the existence, in the lower right part of the diagram and close to the trivial nonfrustrated Cr_2F_5-type quadrant, of two narrow frustrated regions where a Cr_2F_5-type structure is stable. These two bands lie within the type-I region and close to the coordinate axes, with J_3 and J_4 having the same sign, and either J_3 or J_4 being much weaker than J_2. The limits of this area give the boundary within which J_3 and J_4 should lie, whatever the superexchange mechanisms may be, in order to be consistent with the observed magnetic structure of Cr_2F_5. In the next section, we will examine the different coupling mechanisms responsible for interactions J_3 and J_4 and discuss their consistency with the simulation results.

5. Discussion

Let us now detail the mechanisms responsible for the superexchange interactions. The coupling mechanisms corresponding to

J_1, J_2, and J_5 seem to be well understood. The sign (or strength) of these interactions is well established and it is consistent with the magnetic structure determined above. We will only summarize below the arguments developed in Refs. (*13*) and (*14*):

(i) interaction J_1 results from the cancellation of several exchange and superexchange mechanisms, some of them being AF and others F. The weakness of J_1 is confirmed experimentally by the low ordering temperature (<4.2 K) of $CrAlF_5$, which is isostructural to Cr_2F_5 with only J_1-type coupling interactions (*14*);

(ii) interaction J_2 results from 180°-type Cr^{III}–F–Cr^{III} superexchange, often encountered in other chromium fluorides such as CrF_3, $CaCrF_5$ (isostructural to Cr_2F_5), or $KCrF_4$, and unambiguously identified as antiferromagnetic. The superexchange mechanism involved in this interaction is of the π-type between half-filled t_{2g} Cr^{III} orbitals;

(iii) interaction J_5 is of the same type as interaction J_2, involving half-filled t_{2g} orbitals of Cr^{II} and Cr^{III} cations.

Problematic interactions J_3 and J_4 involve two Cr^{II} and one Cr^{III} cations located at the vertices of a triangle whose center is occupied by a fluorine anion (F2). The coupling mechanisms will greatly depend on the possibility of overlapping between the *p* orbitals of fluorine and the *d* orbitals of the cations. The orientation of the *d* orbitals of the cations is fairly well defined: e_g orbitals are pointing approximately toward the apices of coordination octahedra (half-filled d_{z^2} Cr^{II} orbital defines the long Cr^{II}–F distance), while t_{2g} orbitals are directed toward the middle of the edges of the octahedra. The situation concerning fluorine *p* orbitals is less clear. One can expect one of these orbitals to be orthogonal to the Cr_3F triangle, thus being parallel to the **b** axis of the structure. Such a configuration has been shown to be energetically favorable in rutiles (*22*). The exact position of the two other *p* orbitals in the (**a, c**) plane is not known, although Osmond proposed a probable orientation giving the best overlap with the *d* orbitals of the three chromium cations linked to F2 (*13*). We examined different orientations of these orbitals in the (**a, c**) plane and checked the resulting overlaps. It appears that, if the strength (or even the existence) of some mechanisms can be sensitive to the direction of the *p* orbitals of F2, the resulting component on the coupling constant should not be too greatly influenced. Our main qualitative conclusions are therefore expected to be rather independent from the orientation of the *p* orbitals of F2 in the (**a, c**) plane.

Before examining successively each interaction J_3 and J_4, we would like to stress a point that could be at the origin of some misinterpretation in previous works. Within the Cr_3F triangle, Cr^{II}–F–Cr^{III} superexchange angles are far from 180°; reference to coupling mechanisms which are characteristic of 180°-type configuration only could be confusing and misleading. Interactions J_3 and J_4, with 120° and 130° superexchange angles, respectively, should most likely be considered as examples of the "intermediate-angle cation–anion–cation interactions" evoked in Ref. (*6*), p. 183. Therefore, more complicated mechanisms, where 90°- and 180°-type superexchanges compete, should be taken into account. We will now reconsider interactions J_3 and J_4 on this basis.

In the following, we shall neglect double correlation effects. The main mechanisms described below are illustrated in Fig. 7, where the orientation of the orbitals of F2 corresponds to the model proposed by Osmond.

Interaction J_3

This interaction corresponds to the superexchange Cr^{II}–F–Cr^{III} with a superexchange angle close to 120° and a long Cr^{II}–F distance along the half-filled d_{z^2} orbital of divalent chromium. The mechanism which is likely to yield the largest overlap, what-

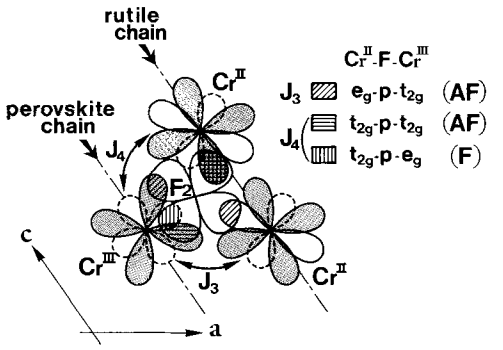

FIG. 7. Orbitals overlap around F2 in Cr_2F_5. Only orbitals in the (**a, c**) plane have been represented according to the following code: dashed line/open, empty e_g orbitals of cations; full line/open, half-filled e_g orbital (d_{z^2}) of Cr^{II} and filled p orbitals of F2; full line/shaded, half-filled t_{2g} orbitals of cations. The main overlaps discussed in the text are highlighted according to the hatching code described in the figure.

ever the in-plane orbital orientation, is $e_g(Cr^{II}, d_{z^2})$–p–$t_{2g}(Cr^{III})$. It is AF by delocalization. Note that such a mechanism would be impossible in a classical 180°-type configuration. This probably explains why it has not been taken into account in previous reports.

The strength of the F interaction $e_g(Cr^{II}, d_{z^2})$–p–$e_g(Cr^{III})$, put forward in Ref. (*14*), is highly dependent on the fluorine orbital orientation. The overlap can even vanish for some orientations, for instance the one proposed by Osmond (see Fig. 7).

The magnetic structure of Cr_2F_5 described in Section 3 is consistent with the predominance of AF e_g–p–t_{2g} on F e_g–p–e_g.

Other interactions, such as t_{2g}–p–e_g (F) or t_{2g}–p–t_{2g} (AF) can also be present for specific p orbital orientations, but they are expected to be much weaker due to a very small orbital overlap. Our conclusion is thereby that J_3 is most likely AF.

Interaction J_4

Antiferromagnetic in-plane t_{2g}–p–t_{2g} and (probably weaker) out-of-plane t_{2g}–$p\pi$–t_{2g} interactions are present whatever the orientation of the fluorine p orbitals may be.

Another interaction, which was neglected in previous reports, is also present independently from the position of fluorine orbitals, namely the ferromagnetic $t_{2g}(Cr^{II})$–p–e_g (Cr^{III}) interaction. Such a mechanism is impossible with a 180°-type atomic configuration, but becomes possible and strengthens when the superexchange angle decreases. It is responsible for the weakening of the global AF interaction with the departure from 180°, which is consistent with the $\cos^2\theta$ dependence (*23–25*) of the interaction strength observed for $3d$ cations (θ = M–X–M angle). Eventually, the sign of the global interaction can even change when θ approaches 90° (*26*).

About the relative strength of the previous mechanisms in Cr_2F_5, clues can be found in other chromium fluorides. As far as e_g orbitals of chromium (II) (and particularly $e_g(d_{z^2})$) are not implied in this interaction, the situation here is comparable to the case of a corresponding Cr^{III}–F–Cr^{III} mechanism. From a previous investigation concerning $\alpha KCrF_4$ (*2*) we already know the evolution of Cr^{III}–F–Cr^{III} coupling intensity with the superexchange angle. The blank angle, that is the angle for which F and AF mechanisms exactly compensate, was found to be about 129.7°. The superexchange angle corresponding to the J_4 interaction (130°) is therefore very close to the blank angle involving chromium (III) cations. Whatever its sign may be, we can thus expect the interaction J_4 in Cr_2F_5 to be very weak, because of the almost complete cancellation of t_{2g}–p–t_{2g} and t_{2g}–p–e_g mechanisms.

In summary, we conclude that in Cr_2F_5, interactions J_2, J_3, and J_5 are antiferromagnetic, while interactions J_1 and J_4, whose sign cannot be ascertained, are most probably very weak. The preponderance of AF interactions is consistent with the large, negative, Curie–Weiss temperature of the compound (θ_c = −95(5) K from Ref. (*14*)). According to the previous considerations, the representative point of Cr_2F_5 in the J_3–J_4 phase diagram should be located in the

shaded oval area of Fig. 6. It belongs to the type-I area of the diagram, therefore it is consistent with the magnetic structure found from neutron diffraction data.

6. Conclusion

We have determined the magnetic structure of Cr_2F_5: it does not correspond to the previously predicted spin configuration. Reexamining the possible superexchange mechanisms and the main orbital overlaps, we found that two out of the three Cr^{II}–F–Cr^{III} interactions were previously misinterpretated. The new mechanisms we propose are consistent with the rules for superexchange interaction and Jahn–Teller distortion; they are also in good agreement with the magnetic structure, as shown by Monte Carlo simulations. The preponderance of antiferromagnetic interactions as predicted by our model is also supported by susceptibility measurements.

Acknowledgments

The authors are very indebted to Mrs. A. M. Mercier for the preparation of the powdered sample of Cr_2F_5.

References

1. P. Lacorre, M. Leblanc, J. Pannetier, and G. Ferey, *J. Magn. Magn. Mater.* **66,** 219 (1987).
2. P. Lacorre, M. Leblanc, J. Pannetier, and G. Ferey, *J. Magn. Magn. Mater.*, **94,** 337 (1991).
3. B. J. Sturm, *Inorg. Chem.* **15,** 672 (1962).
4. H. Steinfink and J. H. Burns, *Acta Crystallogr.* **17,** 823 (1964).
5. V. Scatturin, L. Corliss, N. Elliott, and J. Hastings, *Acta Crystallogr.* **14,** 19 (1961).
6. J. B. Goodenough, "Magnetism and the Chemical Bond," Wiley–Interscience, New York (1963).
7. J. W. Cable, M. K. Wilkinson, and E. O. Wollan, *Phys. Rev.* **118,** 950 (1960).
8. O. Nikotin, P. A. Lindgård, and O. W. Dietrich, *J. Phys.* **C2,** 1168 (1969).
9. M. T. Hutchings, B. D. Rainford, and H. J. Guggenheim, *J. Phys.* **C3,** 307 (1970).
10. E. Belorizky, S. C. Ng, and T. G. Philips, *Phys. Rev.* **181,** 467 (1969).
11. M. T. Hutchings, M. F. Thorpe, R. J. Birgeneau, P. A. Fleury, and H. J. Guggenheim, *Phys. Rev.* **B2,** 1362 (1970).
12. P. Fischer, W. Hälg, D. Schwazenbach, and H. Gamsjäger, *J. Phys. Chem. Solids* **35,** 1683 (1974).
13. W. P. Osmond, *Proc. Phys. Soc.* **87,** 767 (1966).
14. A. Tressaud, J. M. Dance, J. Ravez, J. Portier, P. Hagenmuller, and J. B. Goodenough, *Mater. Res. Bull.* **8,** 1467 (1973).
15. H. M. Rietveld, *J. Appl. Crystallogr.* **2,** 65 (1969).
16. A. W. Hewat, "Harwell Report AERE-R 7350" (1973).
17. L. Koester and H. Rauch, "Summary of Neutron Scattering Lengths," IAEA Contract 2517/RB (1981).
18. R. E. Watson and A. J. Freeman, *Acta Crystallogr.* **14,** 27 (1961).
19. E. F. Bertaut, *in* "Magnetism," (G. T. Rado and H. Suhl, Eds.), Vol. III, p. 149. Academic Press, New York (1963).
20. P. Lacorre, "MCMAG Manual Version 88.01, I.L.L. Technical Report 88LA13T" (1988).
21. P. Lacorre and J. Pannetier, *J. Magn. Magn. Mater.* **71,** 63 (1987).
22. J. K. Burdett, *Inorg. Chem.* **24,** 2244 (1985).
23. C. Boekema, F. van der Woude, and G. A. Sawatzky, *Int. J. Magn.* **3,** 341 (1972).
24. G. A. Sawatzky and F. van der Woude, *J. Phys.* **12,** C6-47 (1974).
25. J. Pebler, W. Massa, H. Lass, and B. Ziegler, *J. Solid State Chem.* **71,** 87 (1987).
26. K. N. Shrivastava, *Phys. Status Solidi (b)* **125,** 441 (1984).